International Journal of Solids and Structures 47 (2010) 2884–2892

Contents lists available at ScienceDirect

International Journal of Solids and Structures

journal homepage: www.elsevier.com/locate/ijsolstr

Analytical model for delamination growth during small mass impact on plates

Robin Olsson *

Swerea SICOMP AB, SE-431 22 Mölndal, Sweden

ARTICLE INFO

Article history:
Received 29 October 2009
Received in revised form 12 May 2010
Available online 22 June 2010

Keywords:
Composite materials
Delamination
Small mass impact
Integral equation
Laminate
Reissner Mindlin plate

ABSTRACT

An analytical model is presented for delamination initiation and growth and the resulting response during small mass impact on orthotropic laminated composite plates, which typically is caused by runway debris and other small objects. The solution is obtained by a fast stepwise numerical solution of a single integral equation. Delamination size, load and deflection history are predicted by extension of an earlier elastic impact model by the author. Good agreement is demonstrated in comparisons with finite element simulations and experiments.

1. Introduction

Impact is a well known concern in composite structures and the effects of impact damage is a major issue in the design of aircraft made of composite materials (Abrate, 1991; Davies and Olsson, 2004). The impact response of plates is governed by the impactor/plate mass ratio, where small mass impactors result in a local response controlled by wave propagation and large mass impactors result in a quasi-static response, Fig. 1 (Olsson, 2000). Small mass impacts result in a more local response with smaller deflections and larger impact loads, and experiments have demonstrated a significantly larger damage for a given impact energy (Olsson, 2000). The mass ratios controlling small and large mass impact response have been discussed by Olsson (2000), who also derived a mass criterion for small mass impact. For central impact on quasi-isotropic plates it is sufficient that the impactor weighs less than 1/4 of the plate.

Contact deformations are often more significant in small mass impact due to the smaller deflections and larger contact loads. Consideration of contact deformations in finite element (FE) models requires use of elastic 3D elements for the plate and impactor, but for computational efficiency FE modellers frequently use shell elements and rigid impactor models. In contrast the current analytical model explicitly includes contact deformations.

There is an abundance of papers on computational models of impact on composites. In recent years simulations using damage or fracture mechanics to consider damage initiation and growth have become increasingly common, but only a few studies have considered realistic laminates with multiple interfaces (e.g. Lopes et al., 2009; Bouvet et al., 2009; Faggiani and Falzon, 2010). The drawback of these methods is the lack of explicit expressions for the influence of various parameters and relatively long computational times (several hours to days). Furthermore, the computational cost increases rapidly with an increasing number of delaminating interfaces. This paper is focused on faster analytical models which are suitable for preliminary design, and are able to cope with an arbitrary number of delaminations without any time penalty.

Before considering delamination growth it is useful to consider previous work on small mass impact on plates without delamination. Small mass impact is independent of the plate boundary conditions and may be treated as an impact on an infinite plate. The effect of a point load on an infinite isotropic plate was first treated by Boussinesq (1885) and subsequently more thoroughly by Sneddon (1945) who also considered flexural stresses and the influence of the size of the loaded area. Small mass elastic impact on isotropic plates without transverse shearing was first treated by Zener (1941) while impact on plates with shearing was considered by Mittal (1987). Small mass impact on orthotropic plates without shearing was treated independently by Frischbier (1987) and Olsson (1989, 1992). The latter model was subsequently extended by Olsson (2002) to include transverse shear in an approximate fashion through generalisation of the approach suggested by Mittal (1987).

The influence of elliptic contact areas resulting from orthotropy and finite contact areas in small mass impact was studied by Mittal and Khalili (1994). More recently plastic contact in small mass impact was studied by Zheng and Binienda (2007). The influence of these complicating factors is, however, usually very small.

The threshold load for a single delamination under large mass (quasi-static) impact conditions was first derived by Davies and Robinson (1992). An exhaustive derivation, using a different

* Tel.: +46 31 706 63 51; fax: +46 31 706 63 63.
E-mail address: robin.olsson@swerea.se

0020-7683/$ - see front matter © 2010 Elsevier Ltd. All rights reserved.
doi:10.1016/j.ijsolstr.2010.06.015

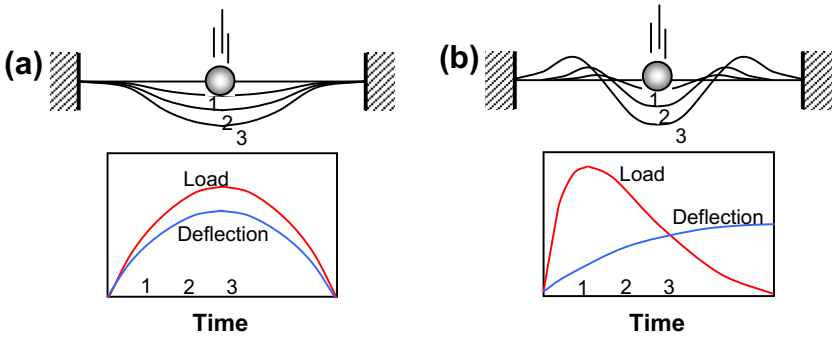

Fig. 1. Comparison between (a) large mass and (b) small mass impact response.

method, with generalisation to an arbitrary number of delaminations was provided by Suemasu and Majima (1996). The corresponding delamination threshold load for small mass impact was derived by Olsson et al. (2006), who also provided an extensive validation and closed form expressions for the resulting delamination threshold velocity.

Analytical models for large mass impact on plates with delamination growth have been presented by Olsson (2001) and Huang et al. (2008), but similar models for small mass impact appear to have been lacking until a solution approach was outlined by Olsson (2009). The current paper gives a more extensive presentation of the approach and also presents some further development of the model.

2. Theory

2.1. Impact response model

Consider a plate of thickness h and density ρ impacted by an elastic concentrated mass M with initial velocity V_0, Fig. 2a, which results in indentation and a contact force F, Fig. 2b. The displacements w_i and w_p of the impactor and plate mass centres have been given by Mittal (1987) and his solution may be rewritten in the following form:

$$\begin{aligned} w_i &= V_0 t - \int_0^t F(\tau)(t-\tau)\,d\tau/M \\ w_p &= \int_0^t \frac{F(\tau)}{4\pi\sqrt{mD_n^*}} \arctan\left[(t-\tau)S_n^*/\sqrt{mD_n^*}\right] d\tau \\ &\quad + \int_0^{t-t_0} \frac{F(\tau)}{2\pi(t-\tau)S_n^*}\,d\tau \end{aligned} \tag{1}$$

Here $m = \rho h$ is the plate mass per unit area, t_0 is a time correction accounting for a finite contact area and D_n^* and S_n^* are effective bending and shear stiffnesses of an orthotropic plate with n delaminations. The original solution by Mittal (1987) did not consider delamination or orthotropic plates and treated D, S and t_0 as constants. In the present solution they are functions of time, and hence have been moved into the integration.

The effective bending stiffness D_n^* of an orthotropic plate with n delaminations is defined as follows (Olsson et al., 2006):

$$\begin{aligned} &D_n^* = D^*/(n+1)^2, \quad \text{where } D^* \approx \sqrt{D_{11}D_{22}(1+\eta)/2} \\ &\text{and} \quad \eta = (D_{12}+2D_{66})/\sqrt{D_{11}D_{22}} \end{aligned} \tag{2}$$

As shown by Olsson (2001), the above expression for D^* is a very close approximation of the exact expression, which involves elliptic functions and was derived in the Appendix of Olsson (1992). Note that the approximation $D^* \approx (1+\eta)/2\sqrt{D_{11}D_{22}}$ used in the main text of Olsson (1992) becomes inaccurate when η not is close to unity.

The effective shear stiffness S_n^* of orthotropic plates with n delaminations has been defined as follows (Olsson et al., 2006):

$$S_n^* = S^*, \quad \text{where } S^* \approx \sqrt{A_{44}^* A_{55}^*} = \sqrt{K_{yz}G_{yz}hK_{xz}G_{xz}h} \tag{3}$$

where K_{xz} and K_{yz} are shear factors, which for laminates with many plies are close to the homogeneous shear factor $K \approx 5/6$ (Whitney, 1973). Thus, S_n^* is independent of n.

The time correction for a finite contact radius c, Fig. 2b, is defined as follows (Olsson, 1992):

$$t_0 = c^2\sqrt{m/D^*}/4 \tag{4}$$

Note that this definition differs from the constant time correction used by Schweiger (1966) and Mittal (1987), as c is a function of time. In essence the correction t_0 expresses the ratio between the contact area and the area affected by transient flexural waves, and may be deduced from the expressions for flexural stresses in the solution by Sneddon (1945).

The contact between a hemispherical impactor of radius R and plate under a load F and indentation approach α is for Hertzian

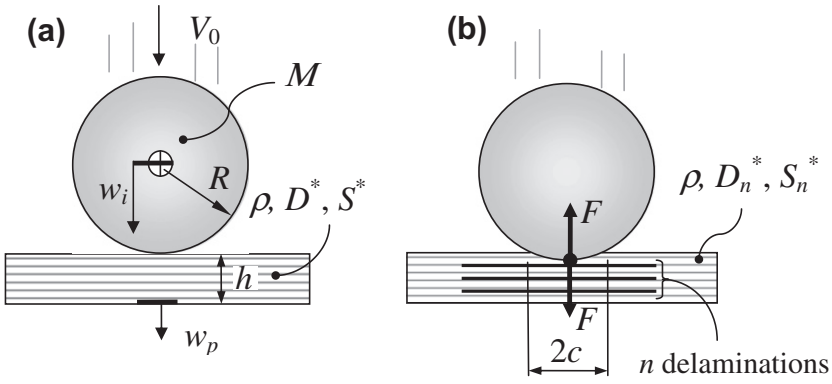

Fig. 2. Impactor (a) before and (b) during indentation of a plate.

(elastic) contact governed by the following relations (where indices i and p refer to impactor and plate):

$$\alpha = w_i - w_p = (F/k_H^*)^{2/3}, \quad \text{where } k_H^* \approx k_H = \frac{4}{3} Q_H \sqrt{R}$$
$$\text{Here} \quad 1/Q_H = 1/Q_i + 1/Q_p \quad \text{and} \quad Q_k \approx E_{zk}/(1 - \nu_{rzk}\nu_{zrk}) \qquad (5)$$
$$k = i, p$$

The expressions k_H^* and k_H are the contact stiffnesses for plates with finite and infinite thickness. More accurate expressions for k_H^* and Q_p of the plate may be found in Olsson et al. (2006). As shown by Goldsmith (1960) the contact radius c, Fig. 2b, under Hertzian contact is given by

$$c = \sqrt{R\alpha} \qquad (6)$$

As a consequence the time constant in Eq. (4) may be written as follows:

$$t_0 = R\alpha\sqrt{m/D^*}/4 \qquad (7)$$

We now introduce the following dimensionless variables (Olsson, 2002):

$$\bar{\alpha} = \alpha/(TV_0), \quad \bar{w}_p = w_p 8\sqrt{mD^*}/(MV_0)$$
$$\lambda_n = (n+1)M/\left(8T\sqrt{mD^*}\right), \quad \beta_n = \sqrt{mD^*}/[(n+1)S^*T]$$
$$\bar{t} = t/T, \quad \bar{t}_0 = t_0/T = k_{tH}\bar{\alpha} \qquad (8)$$
$$\text{where } T = \left[M/(k_\alpha\sqrt{V_0})\right]^{2/5} \quad \text{and} \quad k_{tH} = RV_0\sqrt{m/D^*}/4$$

The dimensionless parameters λ_n and β_n represent the relative mobility in bending and shear. Considering Eqs. (5) and (8) the relations in Eq. (1) may be transformed into the following dimensionless integral equation:

$$\bar{\alpha} = \bar{t} - \int_0^{\bar{t}} \overline{F}(\bar{\tau})(\bar{t} - \bar{\tau})d\bar{\tau} - \bar{w}_p$$
$$\text{where } \overline{F} = \bar{\alpha}^q \quad \text{and} \quad q = 3/2$$
$$\bar{w}_p = \int_0^{\bar{t}} \overline{F}(\bar{\tau})\lambda_n \frac{2}{\pi}\arctan\left[(\bar{t} - \bar{\tau})/\beta_n\right]d\bar{\tau} \qquad (9)$$
$$+ \int_0^{\bar{t}-\bar{t}_0} \overline{F}(\bar{\tau})\lambda_n \frac{2}{\pi}[2\beta_n/(\bar{t} + \bar{t}_0 - \bar{\tau})]d\bar{\tau}$$

For the present Hertzian elastic contact the load exponent was set to $q = 3/2$, while $q \approx 1$ for plastic contact and sandwich panels (Olsson, 2002).

The integral equation in Eq. (9) may be solved numerically by piecewise integration over time increments $\Delta\bar{t}$, assuming a piecewise constant load $\overline{F}$ for each time increment, as suggested by Timoshenko (1913). The resulting stepwise solution becomes:

$$\bar{\alpha}_0 = 0$$
$$\bar{\alpha}_{N+1} = (N+1)\Delta\bar{t} - \frac{1}{2}\Delta\bar{t}^2\sum_{i=0}^{N}\bar{\alpha}_i^q(2N - 2i + 1)$$
$$- \frac{2}{\pi}\sum_{i=0}^{N}\bar{\alpha}_i^q\lambda_n\left[\Delta\bar{t}(N-i+1)\arctan\left\{\frac{N-i+1}{\beta_n}\Delta\bar{t}\right\}\right.$$
$$\left. - \Delta\bar{t}(N-i)\arctan\left\{\frac{N-i}{\beta_n}\Delta\bar{t}\right\}\right. \qquad (10)$$
$$\left. - \frac{1}{2}\beta_n\ln\left\{\frac{\beta_n^2 + (N-i+1)^2\Delta\bar{t}^2}{\beta_n^2 + (N-i)^2\Delta\bar{t}^2}\right\}\right]$$
$$- \frac{4}{\pi}\sum_{i=0}^{N_0}\bar{\alpha}_i^q\lambda_n\beta_n\ln\{(N-i+1)/(N-i)\}$$
$$\text{where } N = \bar{t}/\Delta\bar{t} \quad \text{and} \quad N_0 = (\bar{t} - \bar{t}_0)/\Delta\bar{t} = N - k_{tH}\bar{\alpha}_N/\Delta\bar{t}$$

Note that the parameters λ_n and β_n in the current model change with time as delaminations appear, while they were constants in Olsson (2002). Furthermore, the current model assumes that the parameters λ_n and β_n are fully controlled by the plate properties in the central region with delaminations and that both parameters change instantaneously as delaminations appear.

The numerical solution of Eq. (10) was implemented in a short Fortran 95 program, with a typical run time of a few seconds. Sufficient accuracy was obtained with a dimensionless time step of $\Delta\bar{t} = 0.01$. The program allows onset of a specified number of delaminations nd at a specified dimensionless load $\bar{\alpha}_{dth}^q$. Prior to delamination, n is set to 0, i.e. the values λ_0 and β_0 are used. After delamination onset, n is set to nd, i.e. the values λ_{nd} and β_{nd} are used. For the present Hertzian contact ($q = 3/2$) the dimensionless threshold load is defined by

$$\bar{\alpha}_{dth}^q = (F_{dth}/k_H^*)/(TV_0), \quad \text{where } q = 3/2 \qquad (11)$$

and F_{dth} is the delamination threshold load, defined in Eq. (13).

2.2. Load for delamination onset and growth

The load for growth of n delaminations under small mass impact was defined as follows (Olsson et al., 2006):

$$F_{dn} = C\pi\sqrt{32G_{IIc}D^*/(n+2)},$$
$$\text{where } C = 1/\sqrt{1 - 7\pi^2/216} \approx 1.213 \qquad (12)$$

The above delamination load for small mass impact was obtained by multiplying the corresponding load for large mass impact with the factor C, which accounts for the inertial effects during small mass impact. Delaminations during impact initiate in all interfaces, but a detailed analysis demonstrates that the strain energy release rate is slightly non-uniformly distributed through the thickness (Suemasu and Majima, 1996; Olsson, 2001). Thus, delamination growth first occurs in a single interface ($n = 1$) so that the delamination threshold load F_{dth} at small mass impact is given by

$$F_{dth} = F_{d1} = C\pi\sqrt{32G_{IIc}D^*/3} \qquad (13)$$

This conclusion is supported by extensive experimental evidence both from quasi-static impacts ($C = 1$) (Davies and Robinson, 1992; Olsson, 2001) and from small mass impacts ($C \approx 1.213$) (Olsson et al., 2006). Analysis by Suemasu and Majima (1996) and experimental evidence demonstrate that delamination onset (at F_{d1}) in the most critical interface is followed by more or less uniform delamination growth (at F_{dn}) in all available interfaces.

2.3. Delamination growth model

In the present dynamic case, load and deflection will be out of phase, as illustrated by Fig. 1b. Hence, the conventional linear load–displacement relations from statics are inapplicable. For this reason, delamination growth will be considered during a small

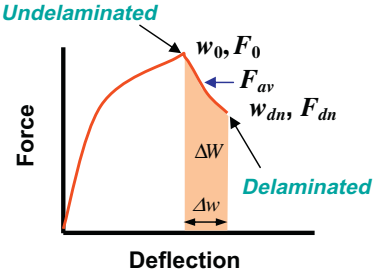

Fig. 3. Load–deflection curve.

portion of the load–deflection curve, where linear relations are assumed to prevail, Fig. 3.

For linear elastic materials the change in external work ΔW is twice the change in the strain energy ΔU. The energy balance during dynamic fracture at a constant strain energy release rate G_c may then be written as follows:

$$G_c A = \Delta W - \Delta U - \Delta T = 2\Delta U - \Delta U - \Delta T = \Delta U(1 - \Delta T/\Delta U) \quad (14)$$

where G_c is the critical strain energy release rate and ΔW, ΔU and ΔT are the changes in external work, elastic energy and kinetic energy due to generation of the crack surface A. The behaviour during delamination growth is schematically illustrated in Fig. 3. Assuming that the load drops linearly, with an average load F_{av}, during the change in deflection Δw from the undelaminated deflection w_0 to the delaminated deflection w_{dn} with n delaminations we may write the change in elastic energy as follows:

$$\Delta U = \frac{1}{2}\Delta W = \frac{1}{2}F_{av}\Delta w = \frac{1}{4}(F_{dn} + F_0)(w_{dn} - w_0) \quad (15)$$

For small mass impact response due to a point load the ratio between the changes in kinetic energy and elastic energy due to delamination is given by (Olsson et al., 2006)

$$\Delta T/\Delta U = 7\pi^2/216 \quad (16)$$

For plates in flexure, delamination takes place under mode II with a critical value G_{IIc} and combination of Eqs. (14)–(16) results in the following approximation of the delamination area, A:

$$A = \frac{1}{4}(F_{dn} + F_0)(w_{dn} - w_0)(1 - 7\pi^2/216)/G_{IIc} \quad (17)$$

The predicted delamination sizes increase to a certain point in the impact history, which is followed by decreasing values of A. Crack healing is not allowed in the current model, and for this reason the delamination area at a given time is defined by the maximum area up to this time. Table 1 presents the ratio between delamination areas predicted from Eq. (17) using the loads and deflections from FE simulations with and without delamination, and the delamination area predicted directly by the FE simulation for various laminates.

These results demonstrate that the delamination size can be predicted with acceptable accuracy, provided that the load and deflection histories can be predicted correctly for plates with and without delaminations.

2.4. Representation of delaminations in real laminates

Delaminations in real impacted laminates are not circular, but consist of peanut shaped delaminations of different orientation (Abrate, 1991; Davies and Olsson, 2004). For large mass (quasi-static) impact the delamination pattern has been thoroughly described (e.g. Hull and Shi, 1993) but a similar pattern has also been observed in small mass impact (Kumar and Rai, 1993). Comparisons between delaminations due to small mass and large mass impact have been presented by Beks (1996) and Morita et al. (1997).

For a laminate with blocked plies and just a few interfaces the individual delaminations are discernible, Fig. 4. For a realistic laminate of equal thickness the individual delaminations are no longer discernible, and the damage zone in a laminate which is quasi-isotropic in flexure appears as more or less circular, Fig. 5

Table 1
Ratio of delamination areas predicted from Eq. (17) and from FE analysis.

h	2 mm	3 mm	4 mm	5 mm	6 mm
A_{theory}/A_{FE}	0.83	0.98	0.98	1.03	0.86

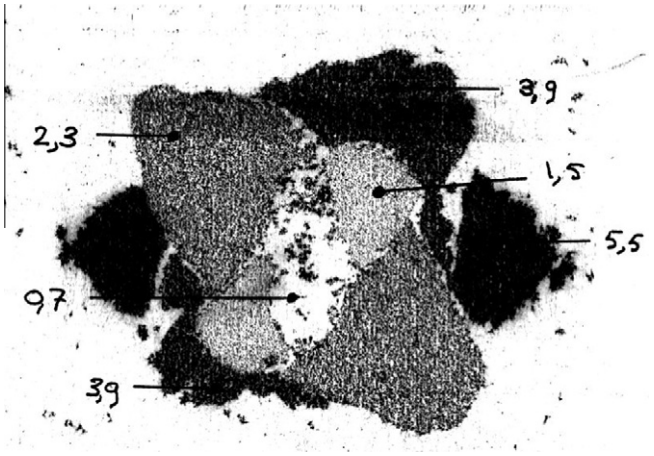

Fig. 4. C-scan of 10 g/10 J impact damage in $[0°_6/90°_6/\pm 45°_6]_s$ blocked laminate (Beks, 1996).

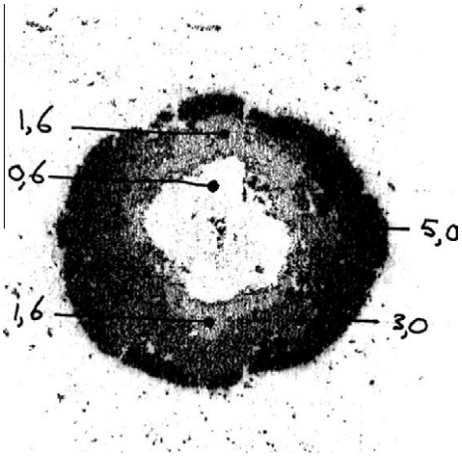

Fig. 5. C-scan of 10 g/10 J impact damage in $[0°/90°/\pm 45°]_{6s}$ standard laminate (Beks, 1996).

$(D_{11}/D_{22} = 1.07)$. The elliptical outer boundary of the damage zone in Fig. 4 is caused by the flexural orthotropy $(D_{11}/D_{22} = 1.68)$ of this laminate. The grey scale in the C-scans of Figs. 4 and 5 indicates increasing depth. Thus, the damage zone may be described as a truncated cone with a base at the unimpacted face of the laminate, as illustrated by the sections in Fig. 6. After the initiation phase the damage zone in thick laminates is often better described as two truncated zones with a common base in the laminate midplane (Davies and Olsson, 2004).

Fractography has demonstrated that $\overline{A} \approx 0.30$ defines the ratio between the delaminated peanut shaped area and an inscribing circular area in quasi-isotropic laminates (Levin, 1991). Delaminations generally appear between all plies of dissimilar orientation, where the size increases with the ply mismatch angle to a maximum at 90° mismatch angle, e.g. +45°/−45° or 0°/90° interfaces (Liu, 1988). The relative delamination area for a mismatch angle of 45°, when compared to a 90° mismatch angle, is $\overline{A}_{45} \approx 0.60$ (Liu, 1988). Thus, the total delamination area in a laminate with multiple peanut shaped delaminations may be represented by n^* equivalent elliptical delaminations of area A^*, half-axes a^* and b^* and average diameter d^*, Fig. 7:

$$A = n^* A^*, \quad \text{where } n^* = \overline{A}\left[\overline{A}_{45} \cdot n_{\Delta 45} + n_{\Delta 90}\right] \quad \text{and}$$
$$A^* = \pi d^{*2}/4 \text{ with } \overline{A} \approx 0.30\ \overline{A}_{45} \approx 0.60\ d^{*2} = 4a^* b^* \quad (18)$$

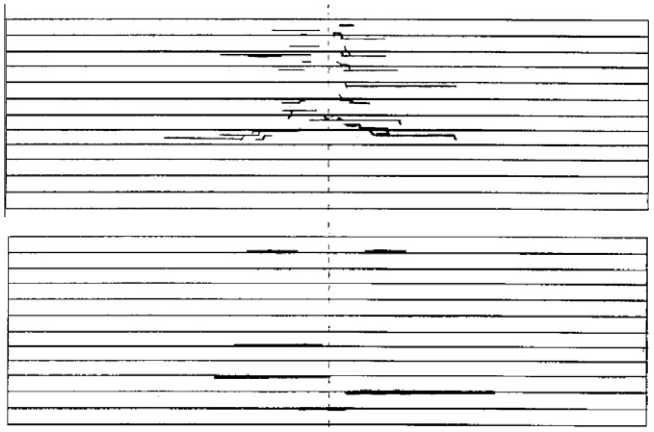

Fig. 6. Perpendicular sections of 10 g/10 J impact damage in $[0^\circ/90^\circ/\pm 45^\circ]_{6s}$ standard laminate (Beks, 1996).

Here $n_{\Delta 45}$ is the number of interfaces with 45° mismatch angle and $n_{\Delta 90}$ the number of interfaces with 90° mismatch angle. In most cases, typical dimensions of delaminations are not uniform through the thickness. It is common that the delamination zone may be described as a truncated cone, with minimum and maximum diameters $d_{\min}$ and $d_{\max}$. The ratio ψ between the average and maximum delamination area is then defined by

$$\begin{aligned}\psi &= A^*/A_{\max} = \frac{1}{n}\sum_{i=1}^{i=n} d_i^2/d_{\max}^2 \\ &= \frac{1}{n}\sum_{i=1}^{i=n} [d_{\min} + (d_{\max} - d_{\min})i/n]^2/d_{\max}^2 \\ \Rightarrow \psi &= \bar{d}_{\min}^2 + \left[(\bar{d}_{\min} - \bar{d}_{\min}^2) + (1-\bar{d}_{\min})^2(2n+1)/6\right](n+1)/n^2 \\ &\text{where } \bar{d}_{\min} = d_{\min}/d_{\max}\end{aligned} \tag{19}$$

Combination of Eqs. (17)–(19) then results in the following expression for the maximum diameter of a conical delamination zone with n^* equivalent delaminations:

$$\begin{aligned}d_{\max} &= d^*\sqrt{A_{\max}/A^*} = d^*/\sqrt{\psi} \\ &\text{where } d^* = \sqrt{4A^*/\pi} = \sqrt{4A/(\pi n^*)} \\ d_{\max} &= \sqrt{(F_{dn}+F_0)(w_{dn}-w_0)(1-7\pi^2/216)/(\pi\psi n^* G_{IIc})}\end{aligned} \tag{20}$$

3. Validation

3.1. Numerical validation

To validate the current analytical model it was first compared with finite element (FE) simulations performed at the delamination threshold velocity for a range of homogenous quasi-isotropic plates with a single delamination developing at the mid-plane. A rigid 3 g ball with 6 mm radius was used to impact 2–6 mm thick plates with properties representative of homogenised quasi-isotropic laminates. The assumed properties have been listed in Table 2.

The FE results of the current paper are based on unpublished data from simulations used for preparation of a previous paper (Olsson et al., 2006). These FE simulations were performed in the explicit code LS-Dyna, using $6 \times 6 \times 3$ single point integration solid elements per mm^3 for the impactor and plate. Contact between the impactor and plate was modelled using sliding-line surface-to-surface contact logic based on the penalty method formulation. Delamination initiation and growth was modelled using a single layer of 0.01 mm thick cohesive (interface) elements at the plate mid-plane interface. The cohesive elements were based on solid elements with cubic stress-displacement decohesion laws accounting for mode mixity and implemented as a user defined material model, as described by Pinho et al. (2006). The approach was based on elements with a bilinear decohesion law by Camanho et al. (2003). The FE simulations confirmed that delamination growth occurred in pure Mode II, as expected. Further details on the FE model may be found in Olsson et al. (2006). No attempt was made here to model growth in multidirectional laminates with multiple orthortropic plies.

Fig. 8 illustrates the analytically predicted behaviour for a 2 mm laminate with (bold line) and without (dotted line) delamination. Delamination onset is reflected by a drop in impact load, and a corresponding increase in deflection. It is noted that the drop in load is significantly larger than the increase in deflections. The difference in load and deflection for the case with and without delamination was used in Eq. (17) to generate predictions of the delamination size.

Fig. 9a–e shows comparisons of the predicted response with delamination by the current analytical model (solid line) and by FE simulations (dashed line). In all cases the delamination growth initiates at the peak (threshold) load with the delamination growing radially from the impact centre and quickly approaching a constant finite size. It is worth noting that the test cases correspond to delamination threshold cases, which were found by gradually increasing the impact velocity by 0.5 m/s in the FE simulations until delamination was achieved.

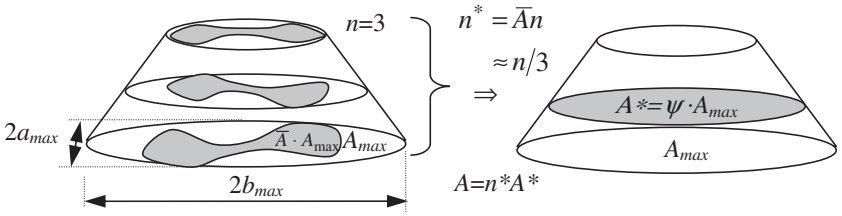

Fig. 7. Real delaminations and equivalent elliptic delamination.

Table 2
Plate properties in finite element simulations.

$E_r = E_x = E_y$	E_z	$G_r = G_{xy}$	$v_r = v_{xy}$	$v_{rz} = v_{xz} = v_{yz}$	τ_U	G_{IIc}	Density ρ
56 GPa	10 GPa	4.5 GPa	0.25	0.25	100 MPa	600 J/m^2	1600 kg/m^3

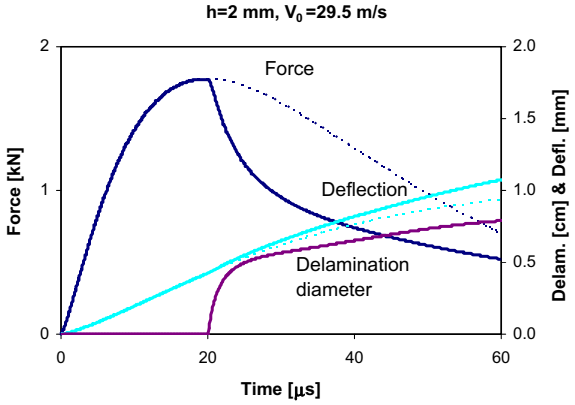

Fig. 8. Analytically predicted response with (solid) and without (dotted) delamination.

3.2. Experimental validation

To experimentally validate the model, it was compared with small mass impact experiments with an instrumented spring-activated 10 g aluminium impactor with 6.35 mm tup radius impacting a 6.22 mm HTA/6376C carbon/epoxy laminate at 10 J, Fig. 10 (Beks, 1996). This energy corresponded to the threshold energy for damage in quasi-static impacts with a 1.5 kg mass, but caused significant delaminations in the small mass impact tests. The $(0^\circ/90^\circ/\pm 45^\circ)_{6s}$ layup consisted of 23 interfaces with 45° mismatch angle and 24 interfaces with 90° mismatch angle, i.e. $n_{\Delta 45} = 23$ and $n_{\Delta 90} = 24$. Thus the expected number of equivalent circular delaminations is $n^* \approx 11$. The damage zone was approximately conical with a ratio $\bar{d}_{\min} \approx 0.41$ between minimum and maximum width. The resulting ratio between average and maximum delamination area is $\psi \approx 0.32$. The measured delamination diameter in this experiment was about 4.5 cm.

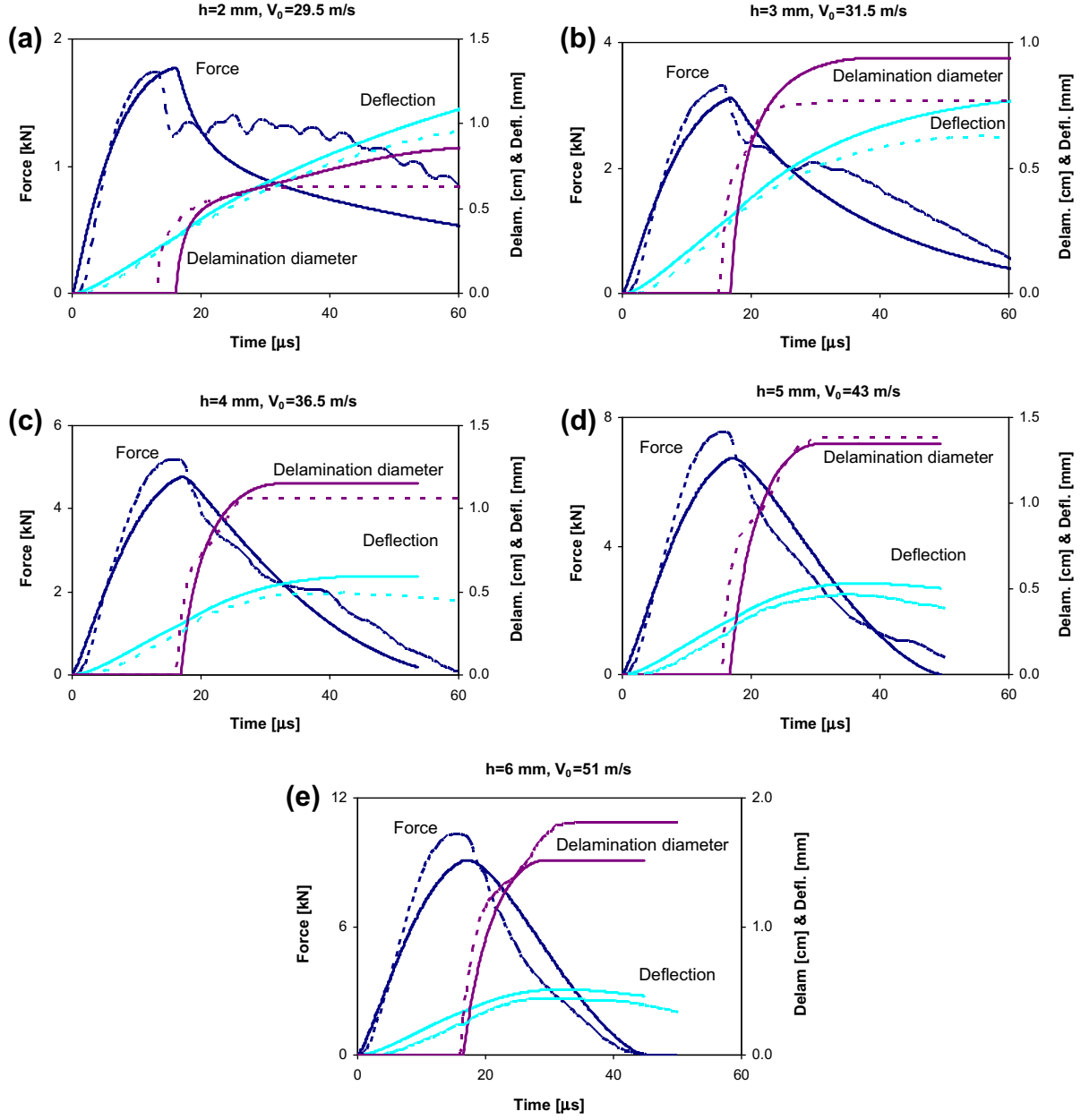

Fig. 9. Comparisons of predictions by analytical model and FE-simulations (solid lines = analytical model, dashed lines = FE-simulation).

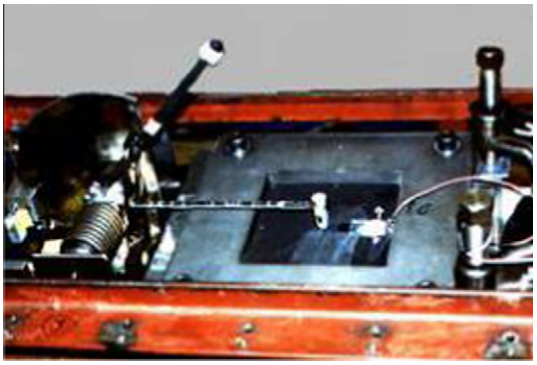

Fig. 10. Spring activated "mouse trap" instrumented impact rig.

In the analysis, the assumed properties of aluminium were $E_i = 70.6$ GPa, $\nu_i = 0.3$ and $\rho_i = 2790$ kg/m^3. Table 3 lists the assumed properties for the HTA/6376C material.

In the experiments, the load was measured by a pair of strain gauges on the impactor. One of these appears as a black rectangle on the cylindrical part of the impactor head in the centre of Fig. 10. The strain gauges had been positioned at a section expected to have virtually uniform stresses. This section had been found by a static FE analysis by Jarlås and Olsson (1997), where it was assumed that the inertial loads could be represented by a uniform mass load. The experimentally measured contact force reported by Beks (1996) was obtained by multiplying the resulting stress with the cross sectional area and a factor accounting for the difference between the mass above the cross section and the total impactor mass. To get a better understanding of the violent oscillations in the impact force measured by Beks (1996) a dynamic FE analysis of an elastic impactor was performed in LS-Dyna for an impact without delamination. The results are shown in Fig. 11 and demonstrate significant differences between the true contact force and the contact force evaluated from the strain gauges. The actual contact force is only 52% of the value estimated from the strain gauge signals and does not show the oscillations observed in the strains, but the reasons for these differences are not yet fully understood. The corrected strain based force was therefore defined as 52% of the nominal value reported by Beks (1996) and the general shape shows good agreement with the actual contact force.

A comparison between predictions and experiment for the expected 11 equivalent delaminations ($n^* = 11$) is presented in Fig. 12, where the corrected strain based force has been used. A fair agreement is observed in the general response, although the predicted delamination size is 33% lower than the size measured in experiments.

Cross-sections of similar specimens impacted quasi-statically at 30 J exhibited delaminations in most of the interfaces (Beks, 1996). The specimens impacted with a small mass at 10 J had only 55% as many delaminations, which were concentrated towards the impacted surface, Fig. 6. To study the influence of the number of delaminations the response was also predicted for 55% of 11 equivalent delaminations, i.e. $n^* = 6$. A comparison between experiment and predictions is given in Fig. 13. The influence of the assumed number of delaminations is relatively moderate although the agreement with experimental response and damage is clearly improved, with a predicted delamination size only 23% lower than in the experiments.

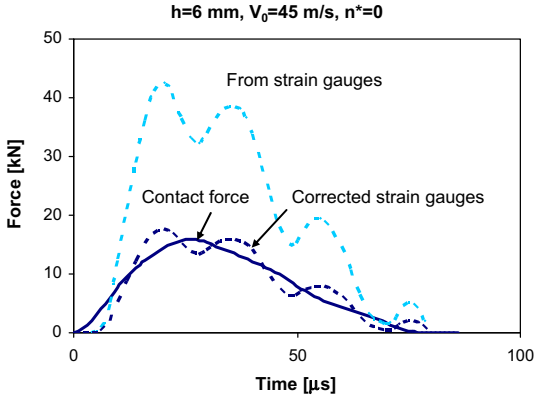

Fig. 11. Comparison of contact force and strain gauge signal in FE-simulation for impact on a plate without delamination growth.

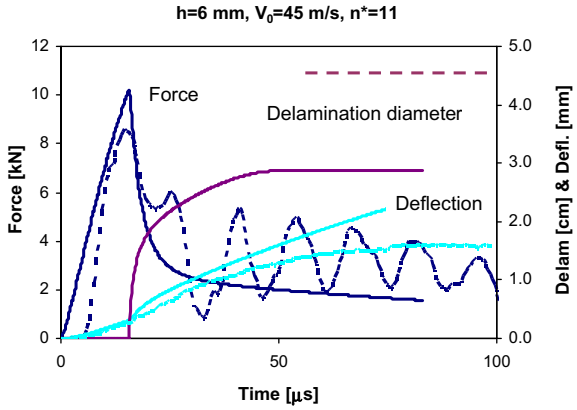

Fig. 12. Comparison between experiments and model for $n^* = 11$ delaminations (solid line = analytical model, dashed line = experiment).

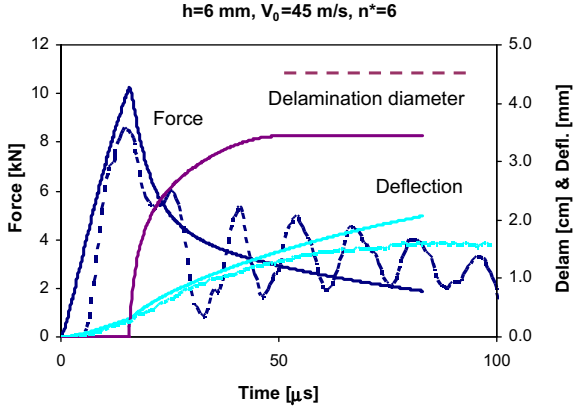

Fig. 13. Comparison between experiments and model for $n^* = 6$ delaminations (solid line = analytical model, dashed line = experiment).

Table 3
Ply properties in experiment.

E_1	$E_2 = E_3$	$G_{12} = G_{13}$	$G_{12} = G_{13}$	$\nu_{12} = \nu_{13}$	ν_{23}	G_{IIc}	Density ρ
137 GPa	10.4 GPa	5.2 GPa	3.9 GPa	0.30	0.5	600 J/m^2	1620 kg/m^3

4. Discussion

The agreement between the predictions by the current model and by FE simulations is very good, considering the significant simplifications made in the analytical model. These simplifications include a linear load–deflection relation during delamination growth and the use of expressions for a fully delaminated plate after delamination onset.

The heuristic assumption of a linear load–displacement relation during delamination growth seems to be justified by the results in Table 1, where the analytically predicted delamination size purely is based on load and displacement data from the FE simulation. The use of a fully delaminated plate to represent the plate after delamination onset implies that the influence of the outer, not yet delaminated, parts of the laminate are neglected. Clearly this is a gross simplification, but the surprisingly good agreement between the analytical predictions and FE simulations indicates that the simplification is acceptable for obtaining an efficient analytical model.

The inclusion of transverse shearing requires consideration of a finite contact area, which is accounted for by the time factor t_0. The corrected treatment of t_0 in the current numerical algorithm was found to significantly reduce the time to peak load, and has virtually eliminated the previously observed phase shift between analytically predicted loads versus experiments and FE simulations (Olsson, 1992, 2002, 2009).

The FE simulations in Fig. 9 were all done just above the delamination threshold velocity, which had been found by gradually increasing the impact velocity by 0.5 m/s. Thus, no delamination was present at velocities just 0.5 m/s less than the ones in Fig. 9. Hence, it may be concluded that noticeable delaminations appear as soon as the delamination threshold velocity has been marginally exceeded.

The comparison with experiments on real laminates with multiple plies of different orientation indicates that the assumed number of equivalent circular delaminations is crucial for reliable predictions of the delamination size. In the small mass impact experiment studied here delaminations were primarily located close to the impacted interface rather than having the assumed uniform distribution over all interfaces. The most probable cause seems to be that the impact velocity was relatively close to the delamination threshold velocity. Similar effects, with a gradual shift from delaminations close to the impacted surface at initiation to fully developed delaminations in all interfaces have been observed in quasi-static impact tests (Davies and Olsson, 2004). Delamination growth is promoted by matrix cracks, and the neglect of such cracks may also have contributed to the underestimated delamination sizes.

The most significant weakness of the model is clearly the simplified representation of the complex damage pattern in real laminates. It should be stressed that this weakness is common with most FE simulations of impact. Full consideration of the complex damage requires capability to model growth of all individual matrix and fibre cracks and delaminations, which requires separate FE elements with progressive damage modelling for *each* ply.

A practical problem in experiments is that the oscillations in recorded strains used to determine loads during small mass impact tests make it difficult to distinguish delamination onset and to compare with model predictions. A way to overcome these problems may be selective filtering after an FFT analysis of the spectral content of the signals. Alternatively loads in the impactor should be measured closer to the point of contact.

5. Conclusions

It has been shown that the suggested analytical model can be used to predict response and delamination size during small mass impact on plates with delamination onset and growth. Noticeable delaminations appear as soon as the delamination threshold velocity has been marginally exceeded.

Acknowledgements

The author is indebted to Dr. Mauricio Donadon who generated the FE simulations in a previous collaboration project (Olsson et al., 2006) and to Dr. Rickard Juntikka for FE-simulation of the experiments with use of an elastic FE model of the impactor.

References

Abrate, S., 1991. Impact on laminated composite materials. Appl. Mech. Rev. 44 (4), 155–190.
Beks, F.-A., 1996. Examination of impact response and damage of composite laminates. FFA TN 1996-29. The Aeronautical Research Institute of Sweden, Bromma, Sweden.
Boussinesq, J.N., 1885. Application des potentiels à l'étude de l'équilibre et du movement des solides élastiques. Gauthier-Villars, Paris. pp. 464–480.
Bouvet, C., Castanié, B., Bizeul, M., Barrau, J.-J., 2009. Low velocity impact modelling in laminate composite panels with discrete interface elements. Int. J. Solids Struct. 46 (14–15), 2809–2821.
Camanho, P.P., Davila, C.G., de Moura, M.F., 2003. Numerical simulation of mixed-mode progressive delamination in composite materials. J. Compos. Mater. 37 (16), 1415–1438.
Davies, G.A.O., Olsson, R., 2004. Impact on composite structures. Aeronaut. J. 108 (1089), 541–563.
Davies, G.A.O., Robinson, P., 1992. Predicting failure by debonding/delamination. In: Debonding/Delamination of Composites. AGARD Conf. Proc. 530. AGARD, Neuilly sur Seine, France, pp. 5-1–5-28.
Faggiani, A., Falzon, B.G., 2010. Predicting low-velocity impact damage on a stiffened composite panel. Composites Part A 41 (6), 737–749.
Frischbier, J., 1987. Theorie der Stossbelastung orthotroper Platten und ihre experimentelle Überprüfung. Mitteilung Nr. 51. Institut für Mechanik, Ruhr-Universität, Bochum, Germany.
Goldsmith, W., 1960. Impact. Edward Arnold, London.
Huang, K., de Boer, A., Akkerman, R., 2008. Analytical modeling of impact resistance and damage tolerance of laminated composite plates. AIAA J. 46 (11), 2760–2772.
Hull, D., Shi, Y.B., 1993. Damage mechanism characterisation in composite damage tolerance investigations. Compos. Struct. 23 (2), 99–120.
Jarlås, R., Olsson, R., 1997. Analysis of equipment used for small mass impact experiments. FFAP H-1291. The Aeronautical Research Institute of Sweden, Bromma, Sweden.
Kumar, P., Rai, B., 1993. Delaminations of barely visible impact damage in CFRP laminates. Compos. Struct. 23 (4), 313–318.
Levin, K., 1991. Characterization of delamination and fibre fractures in carbon reinforced plastics induced from impact. In: Kyoto, Jono M. (Ed.), Mechanical Behaviour of Materials – VI, vol. 1. Pergamon Press, Oxford, pp. 519–524.
Liu, D., 1988. Impact induced delamination – a view of bending stiffness mismatching. J. Compos. Mater. 22 (7), 674–692.
Lopes, C.S., Camanho, P.P., Gürdal, Z., Maimí, P., González, E.V., 2009. Low-velocity impact damage on dispersed stacking sequence laminates. Part II: Numerical simulations. Compos. Sci. Technol. 69 (7–8), 937–947.
Morita, H., Adachi, T., Tateishi, Y., Matsumoto, H., 1997. Characterization of impact damage resistance of CF/PEEK and CF/toughened epoxy laminates under low and high velocity impact tests. J. Reinf. Plast. Compos. 16 (2), 131–143.
Mittal, R.K., 1987. A simplified analysis of the effect of transverse shear on the response of elastic plates to impact loading. Int. J. Solids Struct. 23 (8), 1191–1203.
Mittal, R.K., Khalili, M.R., 1994. Analysis of impact of a moving body on an orthotropic elastic plate. AIAA J. 32 (4), 850–856.
Olsson, R., 1989. Impact response of orthotropic composite plates predicted by a one-parameter differential equation. FFA TN 1989-07. The Aeronautical Research Institute of Sweden, Bromma, Sweden.
Olsson, R., 1992. Impact response of orthotropic composite laminates predicted from a one-parameter differential equation. AIAA J. 30 (6), 1587–1596.
Olsson, R., 2000. Mass criterion for wave controlled impact response of composite plates. Composites Part A 31 (8), 879–887 (Corrigendum in Composites Part A 2001;32(2):291).
Olsson, R., 2001. Analytical prediction of large mass impact damage in composite laminates. Composites Part A 32 (9), 1207–1215.
Olsson, R., 2002. Engineering method for prediction of impact response and damage in sandwich panels. J. Sandwich Struct. Mater. 4 (1), 3–29.
Olsson, R., 2009. Analytical model for small mass impact with delamination growth. In: Proc. 17th Int. Conf. Compos. Mater., Edinburgh.
Olsson, R., Donadon, M.V., Falzon, B.G., 2006. Delamination threshold load for dynamic impact on plates. Int. J. Solids Struct. 43 (10), 3124–3141.
Pinho, S.T., Iannucci, L., Robinson, P., 2006. Formulation and implementation of decohesion elements in an explicit finite element code. Composites Part A 37 (5), 778–789.

Schweiger, H., 1966. Maximale Beansprochung schlagartig belasteter elastischer Platten. DLR FB 66-33. Deutsche Versuchsanstalt für Luft- und Raumfahrt, Mülheim, Germany.
Sneddon, I.N., 1945. The symmetrical vibrations of a thin elastic plate. Proc. Camb. Philos. Soc. 41 (1), 27–43.
Suemasu, H., Majima, O., 1996. Multiple delaminations and their severity in circular axisymmetric plates subjected to transverse loading. J. Compos. Mater. 30 (4), 441–453.
Timoshenko, S.P., 1913. Zür Frage nach den Wirkung eines Stoßes auf einem Balken. Z. Math. Phys. 62, 198–209.
Whitney, J.M., 1973. Shear correction factors for orthotropic laminates under static load. Trans. ASME, J. Appl. Mech. 40 (1), 302–304.
Zener, C., 1941. The intrinsic inelasticity of large plates. Phys. Rev. 59, 669–673.
Zheng, D., Binienda, W.K., 2007. Effect of permanent indentation on the delamination threshold for small mass impact on plates. Int. J. Solids Struct. 44 (25–26), 8143–8158.